

# Synchronization and enhanced catalysis of mechanically coupled enzymes

Jaime Agudo-Canalejo,<sup>1</sup> Tunrayo Adeleke-Larodo,<sup>2</sup> Pierre Illien,<sup>3</sup> and Ramin Golestanian<sup>1,2</sup>

<sup>1</sup>*Department of Living Matter Physics, Max Planck Institute for Dynamics and Self-Organization, D-37077 Göttingen, Germany*

<sup>2</sup>*Rudolf Peierls Centre for Theoretical Physics, University of Oxford, Oxford OX1 3PU, United Kingdom*

<sup>3</sup>*Sorbonne Université, CNRS, Laboratoire Physicochimie des Electrolytes et Nanosystèmes Interfaciaux (PHENIX), UMR 8234, 4 place Jussieu, 75005 Paris, France*

(Dated: October 7, 2021)

We examine the stochastic dynamics of two enzymes that are mechanically coupled to each other e.g. through an elastic substrate or a fluid medium. The enzymes undergo conformational changes during their catalytic cycle, which itself is driven by stochastic steps along a biased chemical free energy landscape. We find conditions under which the enzymes can synchronize their catalytic steps, and discover that the coupling can lead to a significant enhancement in the overall catalytic rate of the enzymes. Both effects can be understood as arising from a global bifurcation in the underlying dynamical system at sufficiently strong coupling. Our findings suggest that despite their molecular scale enzymes can be cooperative and improve their performance in dense metabolic clusters.

*Introduction.*—Since the observation of “the sympathy of two clocks” by Christiaan Huygens in 1665, synchronization phenomena have been observed in a variety of systems, at different time- and length-scales [1–3]. Generic theoretical frameworks, in particular the Kuramoto model, have been widely used to predict the conditions under which synchronization can occur [4]. However, the individual oscillators are usually coupled to each other through a physical medium, and it is often necessary to include the microscopic details of the mechanical coupling between them in order to obtain a useful description. A well-studied example is the synchronization of periodically beating flagella and cilia that are involved in swimming of unicellular organisms and transport of mucus in the respiratory tracts [5, 6]. In the context of simple models that treat the actuating organelles as force monopoles that follow cyclic trajectories, hydrodynamic interactions have been shown to play a crucial role in ciliary coordination [7–12]. Moreover, it has been shown that coupling via elastic stresses in the basal body is important for synchronization in algal flagella [13, 14]. Elastic interactions across the surrounding medium are also known to mediate the synchronization of cardiac cells [15, 16]. In these micro-scale examples, the cyclic motion of each individual oscillator is driven by a non-vanishing, deterministic driving force.

At the even smaller nanoscale, however, molecular motors and enzymes convert chemical energy into mechanical work following repeated thermodynamic cycles [17–21]. These processes take place in a noise-activated regime, where motion only occurs stochastically, in response to barrier-crossing events along a chemical free energy landscape. Recently, the relationship between the conformational changes of enzymes during their catalytic cycle [22, 23] and their stochastic translational dynamics has been the subject of many experimental and theoretical studies [24–33]. While these studies have considered the effect of enzymatic activity on mechanical motion, how mechanical interactions feed back into enzymatic

activity and whether synchronization of the catalytic cycles across enzymes is possible are questions that remain open.

In this Letter, we study the dynamics of two enzymes which undergo conformational changes during their catalytic cycle and interact with each other mechanically. We show that this coupling is sufficient to synchronize their stochastic catalytic steps, and moreover leads to a significant enhancement of their catalytic rate.

*Mechanical coupling.*—We use a minimal model where each enzyme  $\alpha$  is considered to have a single mechanical degree of freedom  $L_\alpha$ , which might represent for example its elongation while undergoing conformational changes; see Fig. 1(a,b). Assuming that the surrounding overdamped medium couples forces to velocities linearly, the dynamics of the elongation of enzyme  $\alpha$  will be governed

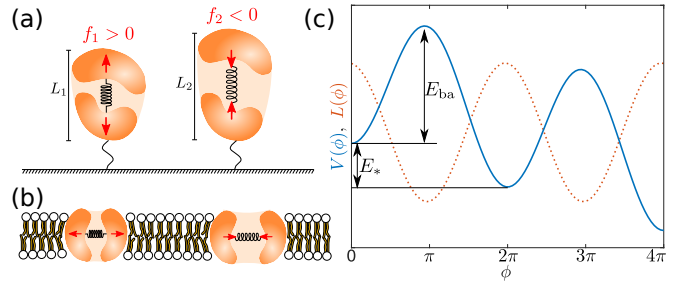


FIG. 1. Examples of mechanical interactions: (a) Two enzymes attached to a surface, each with elongation  $L_\alpha$  and experiencing an internal force  $f_\alpha$ , may interact with each other hydrodynamically through the surrounding viscous fluid medium; (b) Similarly, two enzymes embedded in a lipid membrane might interact elastically. (c) The catalytic cycle of each enzyme is represented by a phase  $\phi_\alpha$  evolving in a biased free energy landscape  $V(\phi)$  (solid blue). The enzyme elongation  $L_\alpha$  tries to adapt to a phase-dependent rest length  $L(\phi)$  (dotted red).

by

$$\dot{L}_\alpha = \mu(f_\alpha + hf_\beta), \quad (1)$$

where  $\mu$  is the mobility associated to the elongation,  $h$  is the (dimensionless) mechanical coupling between the two enzymes  $\alpha$  and  $\beta \neq \alpha$ , and  $f_\alpha$  and  $f_\beta$  are the internal forces (force-dipoles) generated by the corresponding enzymes.

*Mechanochemical coupling.*—We now couple the length dynamics given by Eq. (1) to the chemical cycle that is explored during catalysis, in order to study the effect of mechanical interactions onto the catalytic activity of the enzymes; see Fig. 1(c). We model the state of the chemical reaction happening inside the enzyme using a reaction coordinate  $\phi_\alpha$ . The length  $L_\alpha$  and phase  $\phi_\alpha$  evolve together according to the potential  $U(L_\alpha, \phi_\alpha) = \frac{k}{2}[L_\alpha - L(\phi_\alpha)]^2 + V(\phi_\alpha)$ . Here, the first term describes conformational changes of the enzyme during the catalytic cycle, with  $L(\phi_\alpha)$  being the rest length of the enzyme as a function of the reaction coordinate, and  $k$  the stiffness of the enzyme. The second term represents the free energy of the reaction, described by a biased potential  $V(\phi_\alpha)$  that drives the phase forward [17, 18].

The internal force of an enzyme can then be calculated as  $f_\alpha = -\partial_{L_\alpha} U(L_\alpha, \phi_\alpha) = -k[L_\alpha - L(\phi_\alpha)]$ , which enters the length dynamics in Eq. (1). In turn, the phase dynamics are given by  $\dot{\phi}_\alpha = -\mu_\phi \partial_{\phi_\alpha} U(L_\alpha, \phi_\alpha)$ , where  $\mu_\phi$  is the mobility along the chemical reaction coordinate, resulting in

$$\dot{\phi}_\alpha = -\mu_\phi \{-k[L_\alpha - L(\phi_\alpha)]L'(\phi_\alpha) + V'(\phi_\alpha)\}. \quad (2)$$

Equations (1) and (2) describe the coupled dynamics of length and phase. The dynamics can be simplified further if we assume that the enzyme is very rigid, so that the typical timescale of length relaxations  $(\mu k)^{-1}$  is much shorter than that of changes in the phase velocity. Indeed, the dynamics of the deviation of the length from its preferred value  $\delta L_\alpha \equiv L_\alpha - L(\phi_\alpha)$  is governed by  $L'(\phi_\alpha)\dot{\phi}_\alpha + \delta\dot{L}_\alpha = \dot{L}_\alpha = -\mu k(\delta L_\alpha + h\delta L_\beta)$ . Assuming fast relaxation, we can set  $\delta\dot{L}_\alpha = 0$  and solve for  $\delta L_\alpha$  to obtain  $-\mu k\delta L_\alpha = L'(\phi_\alpha)\dot{\phi}_\alpha - hL'(\phi_\beta)\dot{\phi}_\beta$ , to first order in  $h$ . This shows that there is a difference between the elastic rest length of the enzyme and its dynamical rest length. The non-vanishing deformation leads to a finite force (-dipole) that is present during the enzyme activity.

*Phase equations.*—The above calculation allows us to project the dynamics of the coupled-enzymes system onto the slow manifold of the configuration space defined by the phases  $\phi_\alpha$ . Using the definition  $A_\alpha(\phi_\alpha) \equiv \sqrt{\frac{\mu_\phi}{\mu}} L'(\phi_\alpha)$ , the resulting deterministic dynamics is found as

$$\dot{\phi}_\alpha(t) = \omega(\phi_\alpha(t)) + h \left[ \frac{A_\alpha A_\beta}{1 + A_\alpha^2} \right] \omega(\phi_\beta(t)), \quad (3)$$

to first order in  $h$ , where

$$\omega(\phi_\alpha) = -\frac{\mu_\phi V'(\phi_\alpha)}{1 + A_\alpha(\phi_\alpha)^2}, \quad (4)$$

which demonstrates that the reaction dynamics of two enzymes that undergo conformational changes during catalysis are coupled through the mechanical interaction. Importantly, the dynamics is independent of the stiffness  $k$ , as long as it is large enough for the fast relaxation approximation to hold. We note that in typical Kuramoto-like descriptions the main driving term is either a constant or a positive-definite function of the phase that can be mapped onto a constant using a gauge transformation [4]. In our system, however, the chemical driving force as defined by Eq. (4) vanishes and changes sign twice through a complete catalytic cycle. Moreover, the interaction term is controlled by the same driving force, which makes it distinct from other previously studied models of synchronization.

*Stochastic dynamics.*—Since enzymes operate at the molecular scale, the appropriate description of their dynamics should include stochastic effects. To construct such a description, we will need to coarse-grain the stochastic dynamics of all the relevant degrees of freedom, which can in general be cumbersome. The systematic dimensional reduction of the dynamics in terms of the slow variables and the fact that in this limit  $U(L_\alpha, \phi_\alpha) \simeq V(\phi_\alpha)$ , however, provide a route to constructing the effective stochastic dynamics. To this end, it is convenient to recast Eq. (3) in the form

$$\dot{\phi}_\alpha(t) = M_{\alpha\beta}(\{\phi_\mu\}) [-\mu_\phi V'(\phi_\beta)], \quad (5)$$

where the mobility tensor is defined as  $M_{11} = 1/(1 + A_1^2)$ ,  $M_{22} = 1/(1 + A_2^2)$ , and  $M_{12} = M_{21} = hA_1A_2/[(1 + A_1^2)(1 + A_2^2)]$ , and Einstein summation convention for repeated indices is used. We can now build the stochastic dynamics of the system in form of the corresponding Fokker-Planck equation

$$\partial_t \mathcal{P} = \partial_\alpha \left[ M_{\alpha\beta} \mu_\phi \left( V'(\phi_\beta) \mathcal{P} + k_B T \partial_\beta \mathcal{P} \right) \right], \quad (6)$$

for the probability distribution  $\mathcal{P}(\phi_1, \phi_2, t)$ , which ensures equilibration when the potential  $V(\phi)$  is unbiased.

Note that Eq. (6) belongs to the general class of stochastic systems with multiplicative noise, which implies that building a Langevin dynamics for the system will require special considerations. We first introduce the square-root of the mobility tensor  $\Sigma$  via  $M_{\alpha\beta} = \Sigma_{\alpha\nu} \Sigma_{\beta\nu}$  [34], and then construct the corresponding Langevin equations [associated with Eq. (6)] as follows

$$\begin{aligned} \dot{\phi}_\alpha(t) = & M_{\alpha\beta} [-\mu_\phi V'(\phi_\beta)] + k_B T \mu_\phi \Sigma_{\alpha\nu} \partial_\beta \Sigma_{\beta\nu} \\ & + \sqrt{2k_B T \mu_\phi \Sigma_{\alpha\beta}} \xi_\beta(t), \end{aligned} \quad (7)$$

where  $\xi$  satisfies  $\langle \xi_\alpha(t) \xi_\beta(t') \rangle = \delta_{\alpha\beta} \delta(t - t')$ . In Eq. (7) the Stratonovich convention for the multiplicative noise

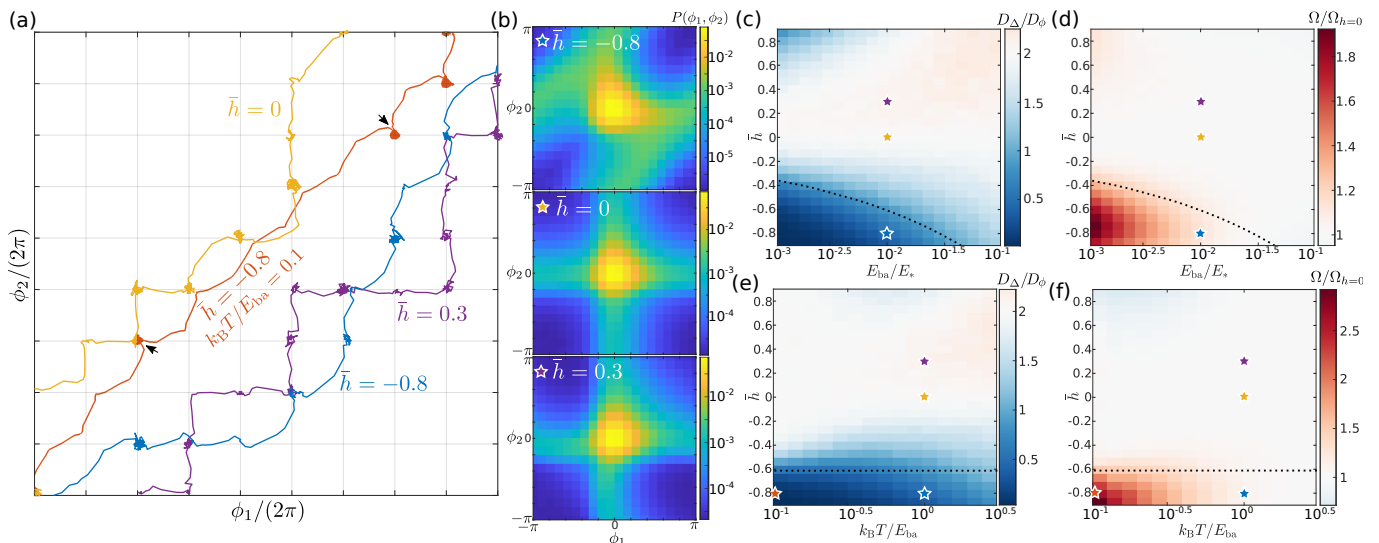


FIG. 2. (a) Trajectories of the system in  $(\phi_1, \phi_2)$  space for different values of  $\bar{h}$ , with  $E_{ba}/E_* = 10^{-2}$  and  $k_B T/E_{ba} = 1$  (except where noted). The grey grid marks integer values of  $\phi_{1,2}/(2\pi)$ . Trajectories for zero or positive coupling show mostly horizontal and vertical segments, implying independent single-enzyme steps, whereas those for negative coupling ( $\bar{h} = -0.8$ ) are diagonal, implying synchronized two-enzyme steps. For  $\bar{h} = -0.8$  and low noise, multi-step diagonal runs are observed (red line, between the two arrows). (b) Probability distribution  $P(\phi_1, \phi_2)$ , with phases modulo  $2\pi$ , for the same trajectories as in (a). Note the diagonal stripes for  $\bar{h} = -0.8$ . (c-f) Heatmaps for the phase-difference diffusion coefficient  $D_\Delta$  (normalized by the single-phase diffusion coefficient  $D_\phi$ ) (c,e) and the catalytic rate  $\Omega$  (normalized by the catalytic rate in the absence of coupling  $\Omega_{h=0}$ ) (d,f), as a function of the bias of the free energy landscape  $E_{ba}/E_*$  and  $\bar{h}$  for fixed noise  $k_B T/E_{ba} = 1$  (c,d), and of the noise  $k_B T/E_{ba} = 1$  and  $\bar{h}$  for fixed bias  $E_{ba}/E_* = 10^{-2}$  (e,f). The dashed lines in (c-f) correspond to the synchronization boundary based on the deterministic phase portraits; see Fig. 3.

is used and a corresponding spurious drift term is introduced. This completes the stochastic formulation of the system of two mechanically coupled enzymes.

*Brownian dynamics simulations.*—In what follows, we model the reaction free energy using a washboard potential  $V(\phi) = -F\phi - v \cos[\phi + \arcsin(F/v)]$ , which has minima at  $\phi = 2\pi n$  for all  $n \in \mathbb{Z}$ . The conformational changes of the enzyme mimic the washboard potential, with the rest length given by  $L(\phi) = L_0 - \ell \cos[\phi + \arcsin(F/v)]$ , so that the extrema of  $V'(\phi)$  coincide with those of  $L'(\phi)$ . Lastly, we consider that  $\mu_\phi \ell^2 \ll \mu$ , so that phase changes rather than conformational changes constitute the bottleneck in the dynamics of the enzyme. We note as well that  $F$  and  $v$  determine the height of the free energy barrier  $E_{ba}$  and the free energy difference of the chemical reaction  $E_*$  [see Fig. 1(c)] through  $E_{ba} = [2\sqrt{1 - (F/v)^2} - (F/v)(\pi - 2 \arcsin(F/v))] v$  and  $E_* = 2\pi F$ . Defining dimensionless time as  $\tau \equiv t\mu_\phi v$ , the system depends only on three dimensionless parameters: the rescaled coupling constant  $\bar{h} \equiv h\mu_\phi \ell^2/\mu$ , the bias of the free energy landscape as determined by  $E_{ba}/E_*$ , and the noise strength  $k_B T/E_{ba}$ .

Results of Brownian dynamics simulations of Eq. (7) are shown in Fig. 2. We find that, while for low or positive coupling  $\bar{h}$  the two enzymes typically undergo in-

dependent catalytic steps, for sufficiently negative  $\bar{h}$  the two enzymes tend to step in synchrony; see Fig. 2(a,b). Remarkably, for sufficiently low noise ( $k_B T/E_{ba} \ll 1$ ), we observe long synchronized runs, in which the two enzymes undergo a large number of joint catalytic steps after a thermal fluctuation kicks them out of a local free energy minimum (and before falling back into a minimum). An example of a 5-step run can be seen between the two black arrows for the red trajectory in Fig. 2(a).

These qualitative differences in the trajectories can have strong quantitative effects in the behaviour of the system over long periods of time. As a measure of synchronization, we use the phase-difference diffusion coefficient  $D_\Delta$ , calculated from the relation  $\langle(\phi_1 - \phi_2)^2\rangle \sim 2D_\Delta t$ . This can be compared to the single-phase diffusion coefficient  $D_\phi$  calculated from  $\langle(\phi_1 - \langle\phi_1\rangle)^2\rangle \sim \langle(\phi_2 - \langle\phi_2\rangle)^2\rangle \sim 2D_\phi t$ . If  $\phi_1$  and  $\phi_2$  were independent variables, we would expect  $D_\Delta/D_\phi = 2$ , as we observe for  $\bar{h} = 0$ . However, we find [see Fig. 2(c,e)] that negative values of  $\bar{h}$  lead to  $D_\Delta/D_\phi < 2$ , implying that synchronous steps are favoured. Synchronization is most pronounced for strong bias ( $E_{ba}/E_* \ll 1$ ) and low noise ( $k_B T/E_{ba} \ll 1$ ). For positive  $\bar{h}$  we find that predominantly  $D_\Delta/D_\phi \gtrsim 2$ , implying in this case that synchronous steps are inhibited.

We then consider the total catalytic activity, i.e. the number of catalytic steps per enzyme per unit time

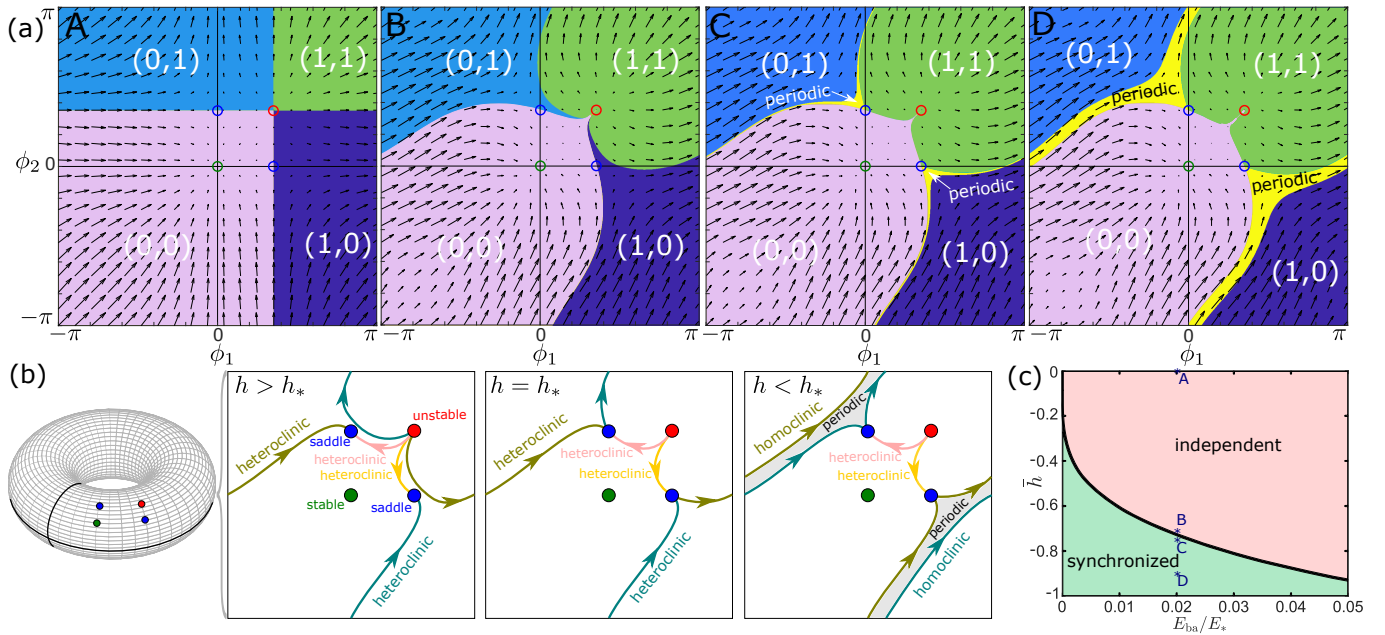


FIG. 3. (a) Phase portraits (basins of attraction) for  $E_{ba}/E_* = 0.02$  and  $\bar{h} = 0, -0.71, -0.75, -0.9$ , corresponding to the points A–D in the phase diagram in (c). Notice the topological transition occurring between B and C. The system always has a stable fixed point [green circle at  $(0,0)$ ], an unstable fixed point [red circle], and two saddle points [blue circles]. For  $\bar{h} > \bar{h}^*$  (A and B), a system initially at  $(0,0)$  will be kicked by fluctuations into the  $(1,0)$  or  $(0,1)$  basins of attraction (blue), leading to an independent single-enzyme step. For  $\bar{h} < \bar{h}^*$  (C and D), however, the system is kicked into either the  $(1,1)$  basin (green), leading to a synchronized two-enzyme step, or into the *running band* of deterministic periodic orbits (yellow), resulting in a run of multiple synchronized two-enzyme steps. (b) The topological transition in the phase portraits can be understood as a global bifurcation of the dynamical system on the torus with decreasing  $h$ . At  $h = h_*$ , two pairs of heteroclinic orbits connecting the unstable point to the saddle points collide. For  $h < h_*$ , two homoclinic orbits arise, with a finite band of periodic orbits between them. (c) Phase diagram based on the topology of the deterministic phase portraits.

over the whole time of the simulation  $\Omega \equiv [\phi_1(\tau_{\text{tot}}) + \phi_2(\tau_{\text{tot}})]/(4\pi\tau_{\text{tot}})$ ; see Fig. 2(d,f). We find that mechanical coupling can enhance catalytic activity, the effect being particularly striking for strongly synchronized cases (with strong bias, low noise, and negative  $\bar{h}$ ), in which case enhancements as large as 200% can be observed, which is a remarkable observation for just two coupled enzymes.

*Phase portrait.*—The fact that synchronization and enhanced catalysis are strongest at low noise suggests that their emergence may be understood from the deterministic phase portraits of the underlying dynamical system in the absence of noise, Eq. (3). Indeed, we find that the dynamical system, which is defined on the torus, undergoes a global bifurcation for sufficiently strong negative coupling  $\bar{h}$ ; see Fig. 3(a,b). Independently of the value of  $\bar{h}$ , the system always has a stable point at  $(0,0)$ , an unstable point at  $(\phi_*, \phi_*)$  where  $\phi_* \equiv \pi - 2 \arcsin(F/v)$  corresponds to the location of the maximum of  $V(\phi)$ , and two saddle points at  $(\phi_*, 0)$  and  $(0, \phi_*)$ . For  $\bar{h} > \bar{h}_*$ , the phase space is divided into four basins of attraction (separated by four heteroclinic orbits), all of which correspond to the stable point  $(0,0)$  but with trajectories that wind differently around the torus on the way there.

At a critical value  $\bar{h} = \bar{h}_*$ , the heteroclinic orbits change topology, and for  $\bar{h} < \bar{h}_*$  two of the heteroclinic orbits become two homoclinic orbits, between which a *running band* of periodic orbits emerges.

This bifurcation has important consequences. Whereas for  $\bar{h} > \bar{h}_*$  thermal fluctuations will typically kick a system which is initially at  $(0,0)$  into either of the basins of attraction corresponding to a single-enzyme step, for  $\bar{h} < \bar{h}_*$  the system is instead kicked into either the basin of attraction corresponding to a synchronized two-enzyme step, or into the *running band*. In the latter case, the system will continue to perform multiple synchronized steps until noise kicks it out of the band once again. The critical value  $\bar{h}_*$  decreases with increasing  $E_{ba}/E_*$ , as seen in Fig. 3(c), and appears to be well described by  $\bar{h}_* \simeq -2(E_{ba}/E_*)^{1/4}$ . The expression for  $\bar{h}_*$  is plotted as the dashed line in Fig. 2(c–f). We observe that it correctly predicts the regions with enhanced synchronization and catalysis.

*Discussion.*—In summary, using a minimal model, we have shown that enzymes that undergo conformational changes during their catalytic cycle can synchronize with each other through mechanical interactions, which moreover can significantly enhance their overall catalytic rate.

Here, synchronization differs qualitatively from that seen in other systems such as generic Kuramoto oscillators or model cilia and flagella, in that the forcing term vanishes at the minima and maxima of the underlying free energy landscape. As a consequence, the motion is driven by thermal noise, and the synchronization arises as an entrainment of the inherently stochastic catalytic steps of the two enzymes. The non-equilibrium mechanism for enhanced catalysis that we observe is also distinct from recent proposals for activated barrier crossing [35–37] which rely on coloured noise.

This work has received support from the Max Planck School Matter to Life and the MaxSynBio Consortium, which are jointly funded by the Federal Ministry of Education and Research (BMBF) of Germany, and the Max Planck Society. T.A.-L. acknowledges the support of an EPSRC Studentship.

- 
- [1] Y. Kuramoto, *Chemical Oscillations, Waves and Turbulence* (Springer, New York, 1984).
- [2] A. Pikovsky, M. Rosenblum, and J. Kurths, *Synchronization* (Cambridge University Press, 2001).
- [3] S. H. Strogatz, *Sync: How order emerges from chaos in the universe, nature, and daily life* (Hachette UK, 2012).
- [4] J. A. Acebrón, L. L. Bonilla, C. J. P. Vicente, F. Ritort, and R. Spigler, The Kuramoto model: A simple paradigm for synchronization phenomena, *Rev. Mod. Phys.* **77**, 137 (2005).
- [5] E. Lauga and T. R. Powers, The hydrodynamics of swimming microorganisms, *Rep. Prog. Phys.* **72**, 096601 (2009).
- [6] R. Golestanian, J. M. Yeomans, and N. Uchida, Hydrodynamic synchronization at low Reynolds number, *Soft Matter* **7**, 3074 (2011).
- [7] A. Vilfan and F. Jülicher, Hydrodynamic flow patterns and synchronization of beating cilia, *Phys. Rev. Lett.* **96**, 058102 (2006).
- [8] N. Uchida and R. Golestanian, Synchronization and collective dynamics in a carpet of microfluidic rotors, *Phys. Rev. Lett.* **104**, 178103 (2010).
- [9] N. Uchida and R. Golestanian, Generic conditions for hydrodynamic synchronization, *Phys. Rev. Lett.* **106**, 058104 (2011).
- [10] N. Uchida, Many-Body Theory of Synchronization by Long-Range Interactions, *Phys. Rev. Lett.* **106**, 064101 (2011).
- [11] N. Uchida and R. Golestanian, Hydrodynamic synchronization between objects with cyclic rigid trajectories., *Eur. Phys. J. E* **35**, 9813 (2012).
- [12] Y. Izumida, H. Kori, and U. Seifert, Energetics of synchronization in coupled oscillators rotating on circular trajectories, *Phys. Rev. E* **94**, 052221 (2016).
- [13] G. Quaranta, M.-E. Aubin-Tam, and D. Tam, Hydrodynamics versus intracellular coupling in the synchronization of eukaryotic flagella, *Phys. Rev. Lett.* **115**, 238101 (2015).
- [14] K. Y. Wan and R. E. Goldstein, Coordinated beating of algal flagella is mediated by basal coupling, *Proc. Natl. Acad. Sci. U.S.A.* **113**, E2784 (2016).
- [15] I. Nitsan, S. Drori, Y. E. Lewis, S. Cohen, and S. Tzili, Mechanical communication in cardiac cell synchronized beating, *Nat. Phys.* **12**, 472 (2016).
- [16] O. Cohen and S. A. Safran, Elastic interactions synchronize beating in cardiomyocytes, *Soft Matter* **12**, 6088 (2016).
- [17] M. O. Magnasco, Molecular combustion motors, *Phys. Rev. Lett.* **72**, 2656 (1994).
- [18] F. Jülicher, A. Ajdari, and J. Prost, Modeling molecular motors, *Rev. Mod. Phys.* **69**, 1269 (1997).
- [19] J. Prost, J. F. Chauwin, L. Peliti, and A. Ajdari, Asymmetric pumping of particles, *Phys. Rev. Lett.* **72**, 2652 (1994).
- [20] N. Golubeva, A. Imparato, and L. Peliti, Efficiency of molecular machines with continuous phase space, *EPL* **97**, 60005 (2012).
- [21] P. Malfaretti, I. Pagonabarraga, and D. Frenkel, Running Faster Together: Huge Speed up of Thermal Ratchets due to Hydrodynamic Coupling, *Phys. Rev. Lett.* **109**, 168101 (2012).
- [22] D. R. Glowacki, J. N. Harvey, and A. J. Mulholland, Taking ockham’s razor to enzyme dynamics and catalysis, *Nat. Chem.* **4**, 169 (2012).
- [23] R. Callender and R. B. Dyer, The dynamical nature of enzymatic catalysis, *Acc. Chem. Res.* **48**, 407 (2015).
- [24] J. P. Günther, M. Börsch, and P. Fischer, Diffusion Measurements of Swimming Enzymes with Fluorescence Correlation Spectroscopy, *Acc. Chem. Res.* **51**, 1911 (2018).
- [25] M. Xu, J. L. Ross, L. Valdez, and A. Sen, Direct single molecule imaging of enhanced enzyme diffusion, *Phys. Rev. Lett.* **123**, 128101 (2019).
- [26] R. Golestanian, Synthetic mechanochemical molecular swimmer, *Phys. Rev. Lett.* **105**, 018103 (2010).
- [27] R. Golestanian, Enhanced diffusion of enzymes that catalyze exothermic reactions, *Phys. Rev. Lett.* **115**, 108102 (2015).
- [28] A. S. Mikhailov and R. Kapral, Hydrodynamic collective effects of active protein machines in solution and lipid bilayers, *Proc. Natl. Acad. Sci. U.S.A.* **112**, E3639 (2015).
- [29] X. Bai and P. G. Wolynes, On the hydrodynamics of swimming enzymes, *J. Chem. Phys.* **143**, 10B616.1 (2015).
- [30] P. Illien, T. Adeleke-Larodo, and R. Golestanian, Diffusion of an enzyme : The role of fluctuation-induced hydrodynamic coupling, *EPL* **119**, 40002 (2017).
- [31] J. Agudo-Canalejo, T. Adeleke-Larodo, P. Illien, and R. Golestanian, Enhanced Diffusion and Chemotaxis at the Nanoscale, *Acc. Chem. Res.* **51**, 2365 (2018).
- [32] Y. Hosaka, S. Komura, and A. S. Mikhailov, Mechanochemical enzymes and protein machines as hydrodynamic force dipoles: the active dimer model, *Soft Matter* **16**, 10734 (2020).
- [33] Y. Koyano, H. Kitahata, and A. S. Mikhailov, Diffusion in crowded colloids of particles cyclically changing their shapes, *EPL* **128**, 40003 (2020).
- [34] To first order in  $h$ , the square-root  $\Sigma$  of the mobility tensor can be written as  $\Sigma_{11} = 1/\sqrt{1+A_1^2}$ ,  $\Sigma_{22} = 1/\sqrt{1+A_2^2}$ ,  $\Sigma_{12} = \Sigma_{21} = hA_1A_2/[\sqrt{1+A_1^2}\sqrt{1+A_2^2}(\sqrt{1+A_1^2} + \sqrt{1+A_2^2})]$ .
- [35] E. Woillez, Y. Zhao, Y. Kafri, V. Lecomte, and J. Tailleur, Activated escape of a self-propelled particle from a metastable state, *Phys. Rev. Lett.* **122**, 258001 (2019).

- (2019).
- [36] E. Woillez, Y. Kafri, and N. S. Gov, Active trap model, *Phys. Rev. Lett.* **124**, 118002 (2020).
- [37] E. Woillez, Y. Kafri, and V. Lecomte, Nonlocal stationary probability distributions and escape rates for an active ornstein–uhlenbeck particle, *J. Stat. Mech.: Theory Exp.* **2020** (6), 063204.